Garnet-based $Li_6CaLa_2Sb_2O_{12}$:Eu^{3+} red phosphors: A potential color-converting material for warm white light-emitting diode

Jiasong Zhong [a], Daqin Chen[a,*], Wenguang Zhao[b], Yan Zhou [a], Hua Yu [a],

Leifeng Chen [a], Zhenguo Ji[a]

[a] College of Materials and Environmental Engineering, Hangzhou Dianzi University,

Hangzhou 310018, China

[b] Ningbo Institute of Material Technology and Engineering, CAS, Ningbo 315201,

China

Abstract: To alleviate the issues of low thermal stability and high correlated color temperature, exploring an inorganic color converter with both yellow- and red-emitting to replace the conventional resin/silicone-based phosphor converter for high-power warm white light-emitting diodes is highly desired so far. In this study, a series of garnet-based $Li_6CaLa_{2-2x}Eu_{2x}Sb_2O_{12}$ (x=0.1~1.0) red phosphors have been successfully synthesized by a conventional high-temperature solid-state method. The microstructure and luminescence properties were systematically investigated by X-ray diffraction, emission/excitation spectra, luminescence lifetimes and temperature-dependent decays. The as-synthesized phosphors exhibited highly efficient red luminescence at 611 nm corresponding to the Eu^{3+} $^5D_0$-$^7F_2$ electric dipole transition, and the luminescence monotonously enhanced as the Eu^{3+} content increasing to 100 mol%. The absence of concentration quenching was ascribed to the large Eu^{3+}-Eu^{3+} distance (7.048~7.105 Å) and subsequently the hampering of the unwanted energy migration among them in the $Li_6CaLa_2Sb_2O_{12}$ crystalline lattice. Impressively, the $Li_6CaLaEuSb_2O_{12}$ phosphor showed excellent thermal stability with

Corresponding authors:
E-Mail: dqchen@hdu.edu.cn (D. Q. Chen)

only 9.7% loss when the recording temperature was raised from 293 K to 553 K. To evaluate the suitability of $Li_6CaLa_2Sb_2O_{12}$:Eu^{3+} as red converter, both the garnet-based $Y_3Al_5O_{12}$:Ce^{3+} yellow phosphors and $Li_6CaLa_2Sb_2O_{12}$:Eu^{3+} red ones co-doped glass ceramics have been successfully fabricated by a low-temperature co-sintering technique. Importantly, the adverse energy transfers between Ce^{3+} and Eu^{3+} are efficiently suppressed due to the spatial separation of Ce^{3+} in $Y_3Al_5O_{12}$ and Eu^{3+} in $Li_6CaLa_2Sb_2O_{12}$ crystal lattice. As a consequence, the quantum yield of the glass ceramic reached as high as 89.3%, and the constructed white light-emitting diode exhibited an optimal luminous efficacy of 101 lm/W, a correlated color temperature of 5449 K and a color rendering index of 73.7. It is expected that the developed $Li_6CaLa_{2-2x}Eu_{2x}Sb_2O_{12}$ red phosphors and the related glass ceramics should have potential applications in the high-power warm white light-emitting diodes.

1. Introduction

Recently, white light-emitting diodes (WLEDs), which are regarded as the next-generation solid-state lighting source, have attracted more and more attention due to their outstanding merits in many aspects such as long operational lifetime, high brightness, low energy consumption and environment friendliness.[1-3] Currently, the commercial WLEDs are mostly fabricated by combining a blue InGaN chip and the yellow-emitting $Y_3Al_5O_{12}$:Ce^{3+} (YAG:Ce^{3+}) phosphors dispersed among organic resin or silicone.[4] However, such approach still has two major drawbacks. Firstly, although YAG:Ce^{3+} possesses many advantages such as a broadband emission in the visible spectral region and excellent chemical and thermal stability,[2,5] in practical application such design will lead to a cool white light with a high correlated color temperature (CCT) and poor color rendering index (CRI) due to the shortage of red-emitting component in the luminescent spectra.[6,7] To solve this issue, it is essential to introduce

red phosphor into the traditional color conversion layer. Therefore, many red phosphors including rare-earth-activated sulfides[8,9] and nitrides[10,11] have been developed to improve the CRI and CCT of WLEDs. However, these red phosphors are not stable or have rigorous synthesis conditions. To overcome these problems, the oxide-based red phosphors are likely to be an alternative choice. Secondly, organic silicone/resin binder in high-power WLEDs is likely to degradation and turns yellow due to the accumulated heat emitted from the high-power blue chip. This will seriously decrease the transmittance of the phosphor-converted layers,[12] and therefore affect the optical performance of WLEDs such as luminance loss and chromaticity shift.[13] In addition, the refractive index of YAG:Ce^{3+} crystal (1.83) is far higher than that of the silicone (1.5), which leads to high light-scattering and low light extraction efficiency.[14] To circumvent these drawbacks, an ideal red phosphor with high thermal stability, low cost and preferable luminescent performance is required; moreover, an inorganic optical material for accommodating both red and yellow phosphors is also demanded.

In recent years, glass-based phosphors, exhibiting unique performance including high thermal conductivity and low thermal expansion coefficient, have been developed for high-temperature resistant WLEDs owing to their much higher thermal stability than silicone.[13,15] Fujita and co-workers have reported the YAG:Ce^{3+} embedded glass ceramic (GC) phosphors for WLEDs, which show excellent thermal properties and moisture resistance.[16-18] However, the fabrication of GC suffers from high temperature (1200-1600 $^{\circ}$C), high cost and low precision. Lately, phosphor in glass (PiG), which is a simple mixture of phosphor powders and inorganic glass powders, has been proved to be a good choice. The glass powders can be transformed into a stable matrix for phosphors under a viscous sintering process.[4, 12, 13, 19-22]

Importantly, PiG exhibits a higher luminous efficiency (LE) and a lower sintering temperature (<800°C).[21,22] In addition, the color coordination can be easily controlled by mixing different phosphors with diverse ratios. Recently, we have reported the fabrication of transparent YAG:Ce^{3+} GC by a PiG route, in which YAG:Ce^{3+} commercial phosphors were mixed with the inorganic TeO_2-based or Sb_2O_3-based glass powders thoroughly and sintered at an optimal temperature.[19,20] The YAG:Ce^{3+} GC-based WLED exhibits excellent optical performance with LE of 124 lm/W, CCT of 6674 K and CRI of 70.[19] However, the high CCT and low CRI for such WLED are still a challenge due to the shortage of red component. Therefore, it is highly desirable to explore a red phosphor with the same structure as YAG, which is advantage for dispersing both red phosphors and YAG:Ce^{3+} yellow ones into the glass matrix and forming transparent glass ceramics.

Garnet-type crystals are considered as the suitable hosts for optical materials due to their stable lattice structure and large heat conductivity.[23,24] Recently, garnet-structured metal oxides with the general formula of $Li_6MLa_2N_2O_{12}$ (M=Ca, Sr, Ba; N=Ta, Sb, Nb) have been extensively studied as the lithium-ion conductors for their chemical and electrochemical stability.[25-27] As an important member, $Li_6CaLa_2Sb_2O_{12}$ (LCLSO) is isostructural with the parent compound $Li_5La_3Sb_2O_{12}$.[28] The crystal double cell of LCLSO viewed from [001] direction is shown in Fig. 1. The Ca^{2+}/La^{3+} are surrounded by eight oxygen atoms and locate in the 24c position of the Ia-3d crystal structure. The Sb^{5+} and Li^+ ions are surrounded by four and three oxygen atoms on the 16a site and 24d or 96h site, respectively.[25] Obviously, $Li_6CaLa_2Sb_2O_{12}$ crystal, exhibiting the same garnet structure as YAG:Ce^{3+} yellow phosphor, should be a suitable host material to accommodate Eu^{3+} for preparing red phosphor owing to the same valence and similar ionic radius between Eu^{3+} (r=1.07 Å,

CN=8) and La^{3+} (r=1.16 Å, CN=8). Eu^{3+} is one of the most interesting rare-earth activators, which can yield red luminescence with high quantum efficiency when doping into an appropriate host.[29] Notably, the red emission of Eu^{3+} mainly originates from the $^5D_0 \rightarrow {}^7F_2$ electric dipole transition, and is highly sensitive to the local chemical environment where Eu^{3+} resides.[30-32]
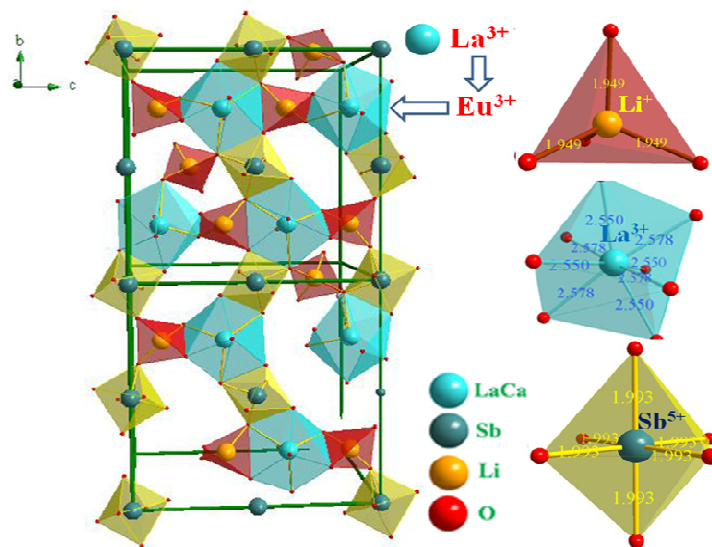
Fig. 1 Simulated crystal structure of $Li_6CaLa_2Sb_2O_{12}$ double cell viewed in [001] direction, and the coordination environment of the $[LiO_4]$ tetrahedral, $[Ca/LaO_8]$ dodecahedral and $[SbO_6]$ octahedral.

Herein, novel $Li_6CaLa_{2-2x}Eu_{2x}Sb_2O_{12}$ (x=0.1~1.0) red phosphors without concentration quenching effect are developed for the first time. Using TeO_2-based glass as host, garnet-type LCLSO: Eu^{3+} and YAG: Ce^{3+} phosphors co-doped GC is fabricated by a PiG route to alleviate the thermal problem and improve CCT/CRI of WLEDs. Importantly, the energy transfers between Ce^{3+} and Eu^{3+} are effectively cut off since Ce^{3+} ions locate in YAG while the Eu^{3+} dopants enter into LCLSO crystalline phase, which results in both intense Ce^{3+} yellow emitting and Eu^{3+} red emitting in the investigated GC. As a consequence, the quantum yield (QY) of the LCLSO: Eu^{3+} and YAG: Ce^{3+} co-doped GC reaches as high as 89.3%, and the GC encapsulated WLEDs

exhibit tunable CCT and CRI, which reveal the prominent feasibility of the red phosphor and the related inorganic glass-ceramic luminescent material in high-power warm WLED applications.

2. Experiment approach

2.1 Sample Preparation

A series of $Li_6CaLa_{2-2x}Eu_{2x}Sb_2O_{12}$ (x=0.1, 0.2, 0.3, 0.4, 0.5, 0.6, 0.8, 1.0) phosphors were prepared by a conventional high-temperature solid-state method. The starting materials of Li_2CO_3 (99.9%), $CaCO_3$ (99.9%), Sb_2O_5 (99.99%), La_2O_3 (99.99%), Eu_2O_3 (99.99%) were weighted in a stoichiometric ratio, and mixed in an agate mortar thoroughly. Then, the homogeneous mixture was transferred to an alumina crucible and calcined in a furnace at 1000 °C for 2h in air.

The precursor glasses with the composition of TeO_2-ZnO-Sb_2O_3-Al_2O_3-B_2O_3-Na_2O were prepared by a conventional melting-quenching technique as previously reported [19]. Then, the as-prepared glass was crushed and milled into glass powders and mixed with 3 wt% commercial Ce: YAG (purchased from XinLi Illuminant Co. LTD.) and 1-15 wt% LCLSO:Eu^{3+} phosphors thoroughly using a ball grinder. Afterwards, the mixture was co-sintered in a platinum crucible at 600 °C for 30 min in the ambient atmosphere. And then, the molten glass was poured into a 300 °C pre-heated copper mold to form the PiG (or GC) composite. In order to relinquish inner stress, the GC composite was further annealed at 230 °C for 12 h and cooled to room temperature naturally. The obtained GC could be easily cut into various shapes and polished for optical characterization.

2.2 Characterization

The purity and structure of the obtained Eu^{3+}-doped LCLSO phosphor and GC samples were determined by powder X-ray diffraction (XRD) analysis, which was

performed on a Bruker D8 diffractometer with CuKa radiation operating at 40 kV and 40mA. The powder XRD data for Rietveld refinement were collected in the range from 15^0 to 120^0 with a steps size of 0.02^0, and the structural refinement was performed using the MAUD program. The microstructures of the GC samples were investigated using a scanning electron microscope (SEM, JSM-6700F, JEOL Ltd., Tokyo, Japan) equipped with an energy dispersive X-ray (EDX) spectroscopy system. Photoluminescence (PL), PL excitation (PLE), temperature-dependent emission spectra and Eu^{3+} decay curves of the products were recorded on a spectrofluoremeter (Edinburgh, FS5) equipped with both continuous (150 W) and pulsed xenon lamps. The Ce^{3+} decay curves of GCs were recorded on a spectrofluoremeter (Edinburgh, FLS920) equipped with a 470 nm picosecond pulsed diode laser (EI-EPL-470). The internal quantum yield (QY) of sample is defined as the ratio of the number of photons emitted to that of photons absorbed, which can be described as the following:

$$\eta = \frac{number\ of\ photons\ emitted}{number\ of\ photons\ absorbed} = \frac{L_{sample}}{E_{reference} - E_{sample}} \qquad (1)$$

Where η represents QY, L_{sample}, $E_{reference}$ and E_{sample} are the emission intensity, the intensities of excitation light without and with the sample in the integrating sphere, respectively. The QYs of the samples were measured on the FS5 spectrofluoremeter equipped with an integrating sphere coated with barium sulfate.

As a proof-of-concept experiment, the WLED device was constructed by encapsulating a GC disk on the blue chip. The sample holder is groove-shaped with the blue chip fixed at the bottom, and the GC was horizontally fastened on the blue chip with opaque silica gel covered around the edge to prevent leakage of blue light. LE, CCT, CRI and Chromaticity coordinate of the GC-based WLEDs were measured in an integrating sphere of 50 cm diameter which was connected to a CCD detector with an optical fiber (HAAS-2000, Everfine Photo-E-Info Co. Ltd).

3. Results and discussion

The phase purity of the as-obtained LCLSO phosphors doped with different contents of Eu^{3+} was investigated by XRD measurements. As shown in Fig. 2a, the XRD peaks of the as-prepared $Li_6CaLa_{2-2x}Eu_{2x}Sb_2O_{12}$ phosphors are similar to those of the standard $Li_5La_3Sb_2O_{12}$ crystal (JCPDS No. 50-0189).[28] The partial substitution of La^{3+} in $Li_5La_3Sb_2O_{12}$ by Li^+ and Ca^{2+} induces the formation of the investigated phosphor structure of $Li_6CaLa_2Sb_2O_{12}$.[33] When La^{3+} ions are completely replaced by Eu^{3+} one, the XRD pattern of the as-prepared $Li_6CaEu_2Sb_2O_{12}$ phosphor is well agreement with that of the standard $Li_5Eu_3Sb_2O_{12}$ crystal (JCPDS No. 50-0187). These results indicates that the Eu^{3+} dopants have been successfully incorporated into the host, and the resulted crystal structure changes from $Li_6CaLa_2Sb_2O_{12}$ to $Li_6CaEu_2Sb_2O_{12}$ with the doping content of Eu^{3+} increasing from 0 to 100 mol%. Figure 2b exhibits the enlarged XRD patterns in the range of $30^0{\sim}40^0$. Evidently, the diffraction peaks gradually shift towards the high-angle direction with increase of Eu^{3+} content, which is attributed to the replacement of the relatively larger $La^{3+}(r=1.16 \text{ Å})$ ions by the smaller $Eu^{3+}(r=1.07 \text{ Å})$ ones.
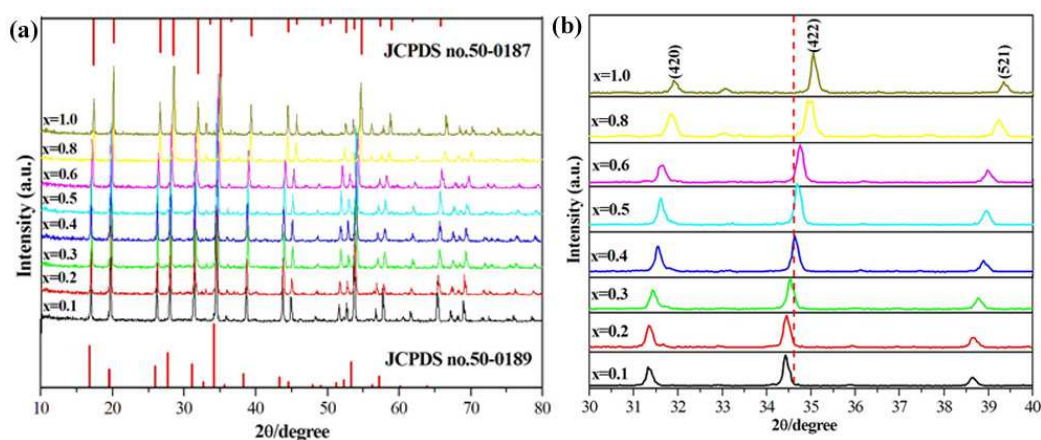
Fig. 2 (a) XRD patterns of $Li_6CaLa_{2-2x}Eu_{2x}Sb_2O_{12}$ (x=0.1, 0.2, 0.3, 0.4, 0.5, 0.6, 0.8, 1.0) phosphors and the standard cubic $Li_5La_3Sb_2O_{12}$ (JCPDS no.50-0189) and $Li_5Eu_3Sb_2O_{12}$ (JCPDS no.50-0187) data; (b) enlarged XRD patterns from 30^0 to 40^0.

The structure refinements of Eu^{3+}-doped LCLSO were carried out using a combination of the Rietveld method and MAUD program. As an example, Fig. 3 exhibits the refinement diffraction pattern of the $Li_6CaLaEuSb_2O_{12}$ sample. The refinement is proceeded by using the structural data of $Li_5La_3Sb_2O_{12}$ given by Cussen and Yip as an initial model.[34] According to the literature,[35] the quality of structural refinement is generally checked by R-values (R_{wnb}, R_b, R_{exp}, R_w, and σ). For the $Li_6CaLaEuSb_2O_{12}$ sample, the R-values of the Rietveld refinement are 5.43%, 6.95%, 3.96%, 2.54% and 2.14 respectively, indicating that the quality of the structural refinement is acceptable.[36] The final refined parameters are list in Table 1. As seen from the Table, the $Li_6CaLaEuSb_2O_{12}$ crystal has the lattice parameters of $a=b=c=12.65\text{Å}$, and the calculated unit cell volume ($V=2024.28$ Å^3) is slightly smaller than that of pure $Li_5La_3Sb_2O_{12}$ ($V=2126.78$ Å^3) crystal[37] since the effective ionic radius of Eu^{3+} (r=1.07 Å) is smaller than that of La^{3+}(r=1.16 Å). This result is well in consistent with the above XRD analysis.
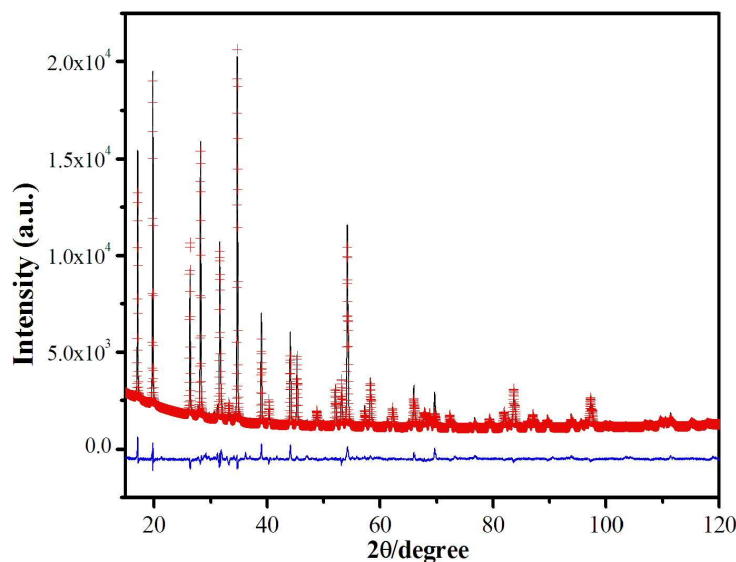
Fig. 3 Representative experimental (crossed) and calculated (red solid line) XRD profiles of $Li_6CaLaEuSbO_{12}$. The difference profile is also provided.

Table 1 Structural parameters of $Li_6CaLaEuSb_2O_{12}$ determined from the XRD data

Atom	Wyckoff	x	y	z	Occupancy	$100U_{iso}/$ Å^2
Li(1)	24d	0.875	0	0.25	0.71(4)	2.1[a]
Li(2)	96h	0.097	0.726	0.607	0.30	0.6[a]
La/Eu	24c	0.125	0	0.25	2/3	1.07(3)
Ca	24c	0.125	0	0.25	1/3	1.07
Sb	16a	0	0	0	1.0	0.93(2)
O	96h	0.275	0.1	0.204	1.0	1.36(3)

[a]U of the Li(1) and Li(2) sites were fixed at those in Ref.[33]

Space Group Ia-3d, a=b=c=12.65Å. R_w = 5.43%, R_{wnb} =6.95%, R_b=3.96%, R_{exp}=2.54% and σ=2.14

PLE spectra of the as-prepared $Li_6CaLa_{2-2x}Eu_{2x}Sb_2O_{12}$ samples with different Eu^{3+} concentration (x=0.1, 0.2, 0.3, 0.4, 0.5, 0.6, 0.8 and 1.0) were recorded by monitoring 611 nm emission, as shown in Fig. 4a. The excitation spectra consist of a broad absorption band in the wavelength range of 250 to 350 nm and several sharp peaks from 350 nm to 500 nm. The broad absorption band is ascribed to O^{2-}—Eu^{3+} charge-transfer (CT) transition, i.e., electron transfer from O^{2-} to Eu^{3+} as Eu^{3+} linked to the O^{2-} ligand.[15] The sharp excitation lines are derived from the f-f transition within the $4f^6$ configuration of Eu^{3+},[38] and two strong absorption bands located at ~393 nm and ~463 nm are assigned to the Eu^{3+} $^7F_0{\rightarrow}^5L_6$ and $^7F_0{\rightarrow}^5D_2$ transition, respectively. Clearly, all the spectra have nearly the same spectral features except that the excitation intensities enhance with increase of Eu^{3+} content. These results indicate that the as-prepared phosphors can strongly absorb the ultraviolet (UV) and blue light, matching well with the output characteristic emissions of UV- and blue- LED.[39]

PL spectra of the corresponding $Li_6CaLa_{2-2x}Eu_{2x}Sb_2O_{12}$ samples under 393 and 463 nm light excitation are shown in Fig. 4b and 4c, respectively. All the emission

spectra exhibit the similar profile and consist of several typical emission bands which are ascribed to the Eu^{3+} transitions from the excited $^5D_0$ level to ^7F_J (J=0, 1, 2, 3 and 4) ones. The strongest emission band locates at 611 nm and corresponds to the Eu^{3+} $^5D_0 \rightarrow ^7F_2$ electric dipole transition.[40] In the PL spectra, the lack of inversion symmetry for Eu^{3+} in LCLSO host results in the dominant $^5D_0 \rightarrow ^7F_2$ transition, which is beneficial to achieving pure red luminescence.[41,42] The dependence of the corresponding PL intensity as a function of Eu^{3+} content is illuminated in Fig. 4d. Impressively, the PL intensity keeps enhancing when Eu^{3+} content increases from 10 mol% to 100 mol%, i.e, the concentration quenching is not observed. In the $Li_6CaLa_2Sb_2O_{12}$ crystal, the mean distance of La^{3+}-O^{2-} is 2.564 Å, and two neighboring $[LaO_8]$ dodecahedral are separated by $[SbO_6]$ octahedral or $[LiO_4]$ tetrahedral, as schematically illustrated in Fig. 1. As a result, the Eu^{3+}-Eu^{3+} distance is quite large (in the range of 7.048~7.105 Å).[28,33,43] It is previously reported that the interaction among Eu^{3+} activators becomes ineffective and the excitation energy migration is hampered when the averages distance among Eu^{3+} ions is larger than 5Å.[15, 44] This means that the probability of non-radiative energy migration between Eu^{3+} ions is greatly reduced in the present host, and therefore the concentration quenching is greatly suppressed. To visualize the Eu^{3+} luminescent enhancement without concentration quenching, photographs of the as-prepared red phosphors, under 393 nm UV light excitation, are provided in Fig. 4e. Evidently, the enhanced luminescence as the Eu^{3+} content increasing from 10 mol% to 100 mol% is clearly visible by the naked eyes.
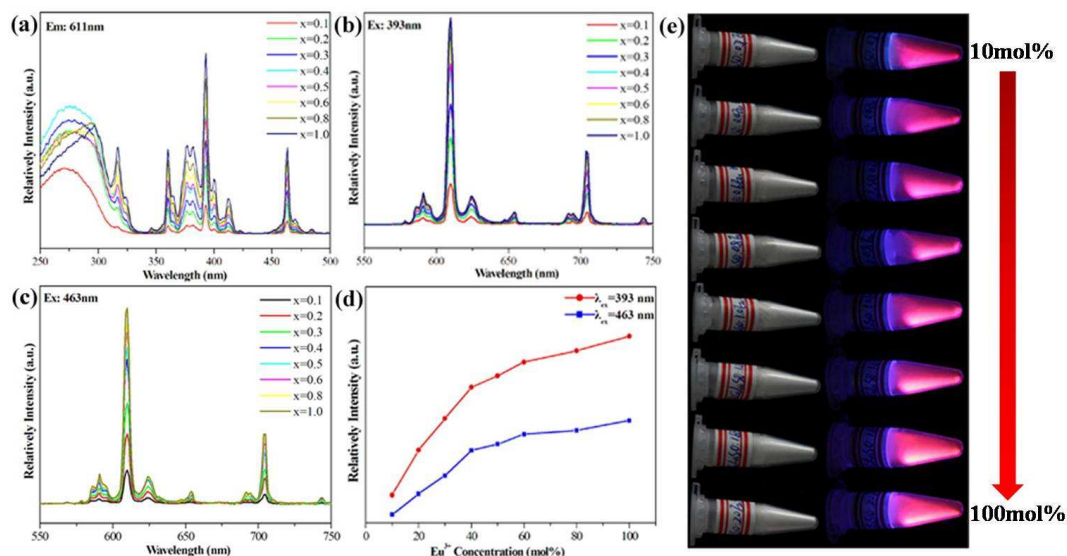
Fig. 4 (a) PLE and (b, c) PL spectra of as-prepared $Li_6CaLa_{2-2x}Eu_{2x}Sb_2O_{12}$(x=0.1~1.0) samples with different Eu^{3+} contents, (d) the corresponding PL intensity as a function of the Eu^{3+} content. (e) Pictures of the red phosphors doped with different Eu^{3+} contents take from the daylight and under the excitation of a 393 nm lamp.

In order to confirm that the concentration quenching does not occur in the Eu^{3+}-doped LCLSO, the luminescent decay behaviors corresponding to Eu^{3+} $^5D_0 \rightarrow ^7F_2$ transition for all the samples were investigated, as exhibited in Fig. 5a. Note that all the samples have the similar decay profiles, which do not obviously vary with Eu^{3+} content. Time-resolved $^5D_0 \rightarrow ^7F_2$ transition shows a single exponential decay even when La^{3+} ions in the host are completely replaced by Eu^{3+} dopants. Therefore, all the decay curves can be well fitted by the single-exponential decay model described by the following equation: [40]

$$I = I_0 \exp\left(\frac{-t}{\tau}\right) \qquad (2)$$

where I and I_0 are the luminescence intensities at time t and 0, respectively, and τ is the radiative decay time. The fitted lifetimes deviate slightly from the average value of 1.06 ms with increase of Eu^{3+} content, as shown in Fig. 5b. Generally, the

non-radiative energy migration among Eu^{3+} ions provides more depopulating channels for Eu^{3+} $^5D_0$ state, and subsequently shortens the fluorescence decay lifetime.[38] However, the lifetime values keep almost the same for all the samples, which further verified that the concentration quenching is absent even when all the La^{3+} ions are substituted by Eu^{3+} ions in LCLSO.
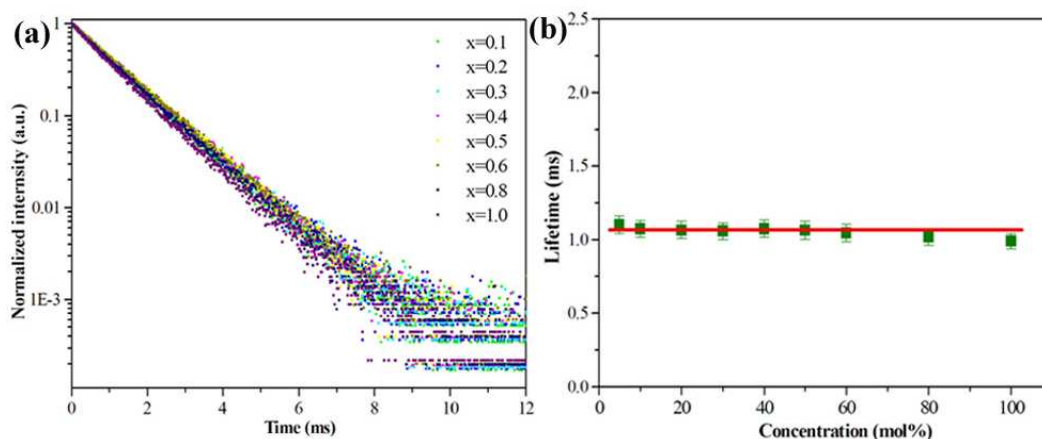
Fig. 5 (a) Decay curves of $^5D_0$ state for the $Li_6CaLa_{2-2x}Eu_{2x}Sb_2O_{12}$ samples upon the excitation of 463 nm by monitoring the 611 nm emission; (b) Decay lifetime of $^5D_0$ state as a function of Eu^{3+} doping content.

For the practical applications, QY and thermal stability of the phosphors are two important factors needing consideration. Using an integrated sphere, the quantitative excitation and emission spectra in the wavelength region of 380-750 nm for the $Li_6CaLaEuSb_2O_{12}$ sample (under 393 nm UV light excitation) were recorded, as exhibited in Fig. 6. Accordingly, the PL QY was calculated to be 41.29%, which is higher than the commercial $Y_2O_3:Eu^{3+}$ phosphor (9.6%, excited by 394 nm UV light)[45] and the previously reported $Sr(La_{0.75}Eu_{0.25})_2Mg_2W_2O_{12}$ (8.8%, excited by 395nm UV light),[45] $Y_2O_2S:Eu^{3+}$ (35%, excited by 317 nm light)[46] as well as $YVO_4:Eu^{3+}$ (38%, excited by 280 nm light).[47] On the other hand, the thermal stability of phosphor has great impact on the light output and color-rendering index of $WLEDs$[48]. Herein, the thermal stability of the red emitting of Eu^{3+} ions in

$Li_6CaLaEuSb_2O_{12}$ is investigated by the luminescence decays recorded under various temperatures. Generally, the emission intensity weakens with increase of the recording temperature. As a result, Eu^{3+} ions exhibit shorter decay lifetime at the higher temperature, and the transition probability is proportional to τ^{-1} (τ is the lifetime) for the Eu^{3+} emitting.[49,50] Therefore, the thermal stability of a luminescence transition process can be expressed by the temperature dependent decay behaviors. As revealed in Fig. 7, all the decay curves keep the single-exponential behavior at the temperature range of 293~553 K and can be well fitted by Equation 2. The lifetime values decrease slightly from 1.089 ms to 0.983 ms as the temperature increasing from 293 K to 553 K. Impressively, only 9.7% loss is observed at the high temperature of 553 K (280 °C), confirming the excellent thermal stability of the investigated red phosphor. These results demonstrate that the as-obtained red phosphor is a potential color converter for high-powder warm WLEDs.
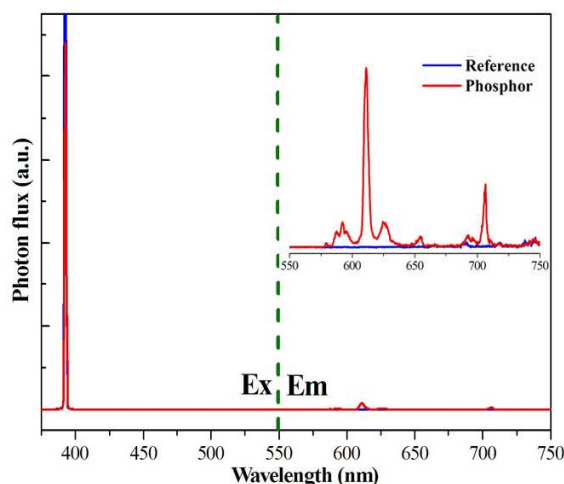
Fig. 6 Excitation and emission spectra of the $Li_6CaLaEuSb_2O_{12}$ and reference samples recorded by a spectrofluoremeter equipped with an integrating sphere for QE measurement. The inset shows the magnified emission spectra in the wavelength range of 500-750 nm.
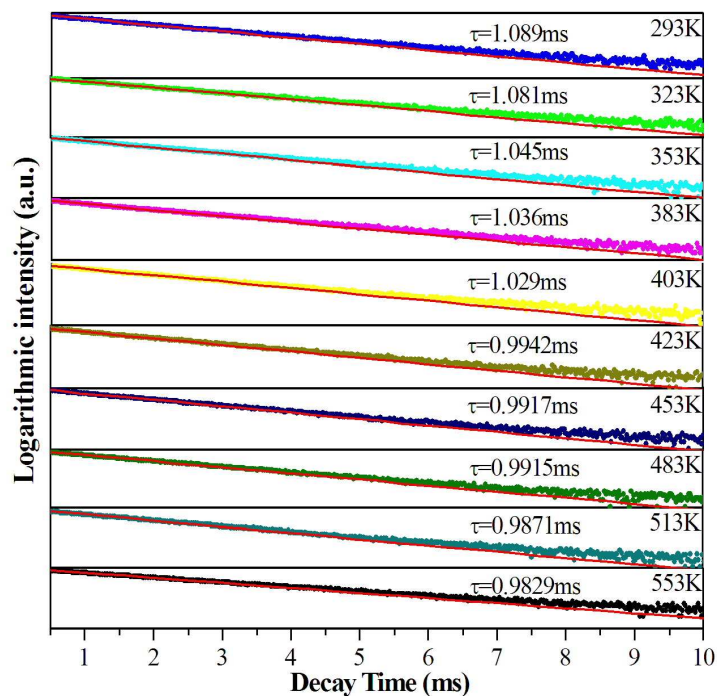
Fig. 7 Decay curves of the Eu^{3+}:$^5D_0 \rightarrow ^7F_1$ transition for the $Li_6CaLaEuSb_2O_{12}$ red phosphor under various recording temperatures

Currently, the commercial WLEDs are usually fabricated using the organic silicone or resin to disperse YAG:Ce^{3+} phosphors, which could not stand the heat or other deteriorating factors due to its low thermal stability. Meanwhile, such fabricated WLED exhibits cool white light with a high CCT and poor CRI due to the lack of red component. Therefore, in order to check the practicality of the fabricated LCLSO:Eu^{3+} red phosphor as color converter for high-power warm WLEDs, we introduced it into the YAG:Ce^{3+} PiG[19] to solve the problem of red deficiency of the product. The crystals structure of the YAG:Ce^{3+} single-doped GC, LCLSO:Eu^{3+} single-doped GC as well as YAG:Ce^{3+} and LCLSO:Eu^{3+} co-doped GC fabricated under a low co-sintering temperature of 600 ^{o}C are shown in Fig. 8. Only a pure YAG crystalline diffraction peaks and the amorphous hump originated from glass matrix are indentified in the YAG:Ce^{3+} single-doped GC, as shown in Fig. 8a. As for the LCLSO:Eu^{3+} single-doped GC, an identical diffraction pattern of LCLSO crystal is

detected (Fig. 8b), indicating that LCLSO:Eu^{3+} phosphors can be introduced into the glass matrix by the low-temperature co-sintering route. Evidently, the diffraction peaks in the YAG:Ce^{3+} and LCLSO:Eu^{3+} co-doped GC shown in Fig. 8c can be easily indexed to YAG and LCLSO crystal phases. These results confirm that both YAG:Ce^{3+} yellow phosphors and LCLSO:Eu^{3+} red ones have been successfully dispersed in the glass matrix, and the degradation of the YAG:Ce^{3+} and LCLSO:Eu^{3+} phosphors is negligible ascribing to the low co-sintering temperature (600 $^{\circ}$C).
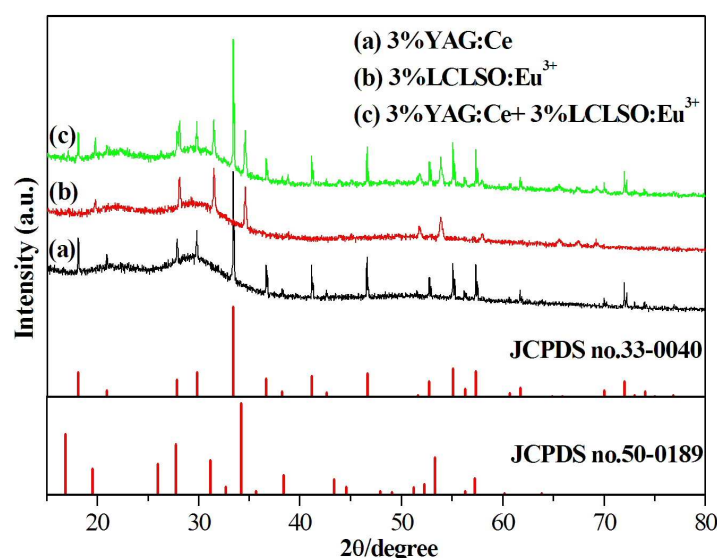
Fig. 8 XRD patterns of (a) the YAG:Ce^{3+} single-doped GC, (b) LCLSO:Eu^{3+} single-doped GC, and (c) YAG:Ce^{3+} and LCLSO:Eu^{3+} co-doped GC. The standard cubic Li$_5$La$_3$Sb$_2$O$_{12}$ crystal (JCPDS no.50-0189) and cubic Y$_3$Al$_5$O$_{12}$ crystal (JCPDS no.33-0040) data are also provided.

Fig. 9a shows SEM image of the LCLSO:Eu^{3+} and YAG:Ce^{3+} co-doped GC sample. The yellow and red circles in the figure represent the phosphor particles of YAG:Ce^{3+} and LCLSO:Eu^{3+}, respectively. Clearly, these phosphor particles with diameters 10-20 μm homogeneously dispersed among the glass matrix without any evident pores. The magnified image (Fig. 9b-9c) evidences the coexistence of a LCLSO:Eu^{3+} particle and a YAG:Ce^{3+} one in the glass matrix. The EDX spectra distinctly demonstrate the characteristic compositions of glass matrix (inset of Fig.9b),

LCLSO:Eu^{3+} (inset of Fig. 9c) and YAG:Ce^{3+} (inset of Fig. 9d) particles. From the

EDX line analyses, Te and Zn elements are detected in glass matrix; Sb, La and Eu

are observed in the LCLSO:Eu^{3+} particle (white region marked by red circle), while Y

and Al elements are recorded in the YAG:Ce^{3+} particle (black region marked by

yellow circle). These results are well agreement with the above XRD results.
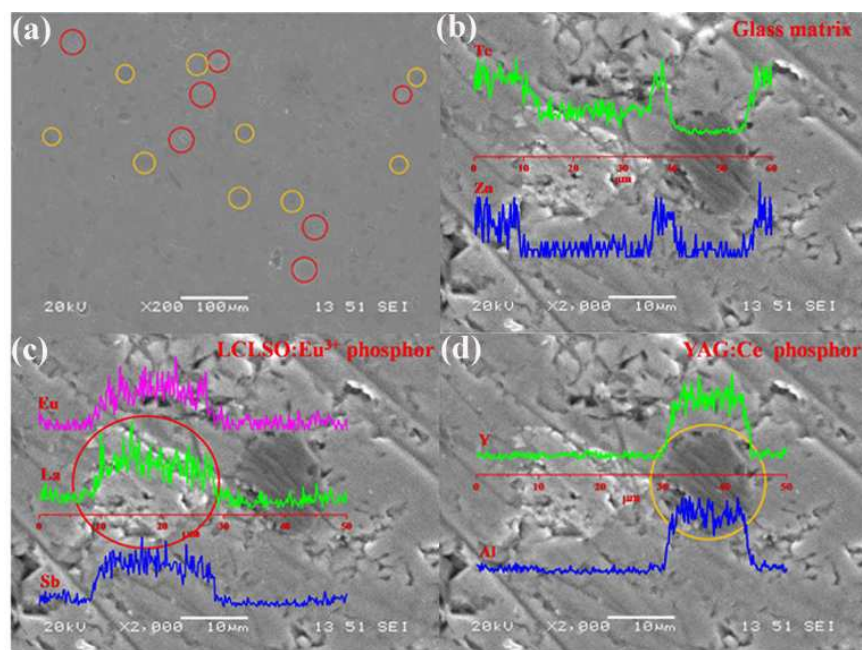
Fig. 9 (a) SEM image of particles in glass matrix; yellow and red circles represent YAG:Ce^{3+} and

LCLSO:Eu^{3+} particles, respectively. (b-d) Magnified image shown in (a), insets are the EDX line

scanning profiles across (b) glass matrix, (c) LCLSO:Eu^{3+} particle and (d) YAG:Ce^{3+} particle.

PLE and PL spectra of the YAG:Ce^{3+} single-doped GC, LCLSO:Eu^{3+}

single-doped GC, and YAG:Ce^{3+} and LCLSO:Eu^{3+} co-doped GC are presented in

Fig.10a. Under 463nm excitation, PL spectrum of the YAG:Ce^{3+} single-doped GC

exhibits a typical Ce^{3+}: 5d→4f broadband emission centered at ~550 nm (Fig. 10a),

which is similar to the case of YAG:Ce^{3+} powders. The corresponding PLE spectrum

of the sample shows two excitation bands centered at ~340 nm and ~460 nm,

respectively, originating from 4f→5d absorption transition of Ce^{3+} ions. It should be

noticed that the excitation intensity at 340 nm is quite weak, which is due to the

absorption influence of the TeO_2-based glass host in the short wavelength region.[19] As for the LCLSO:Eu^{3+} single-doped GC, the PLE spectrum (Fig. 10a), recorded by monitoring the $^5D_0 \rightarrow ^7F_2$ transition of Eu^{3+} at 611 nm, consists of several sharp absorption bands owing to the characteristic intra-configuration 4f-4f transitions of Eu^{3+}. Two dominant absorption bands located at 393 nm and 463 nm are assigned to $^7F_0 \rightarrow ^5L_6$ and $^7F_0 \rightarrow ^5D_2$, respectively. The corresponding PL spectrum, under 463 nm excitation, exhibits a dominant red emission band (611 nm), which is originated from Eu^{3+} $^5D_0 \rightarrow ^7F_2$ electric-dipole transition. From the PLE and PL spectra of the YAG:Ce^{3+} and LCLSO:Eu^{3+} co-doped GC, it is clearly recognized that the excitation and emission bands identified with the $^7F_0$-^5D_J, $^7F_0$-^5L_J and $^5D_0$ -^7F_J transitions of Eu^{3+} locate on the broad excitation and emission bands of Ce^{3+} (Fig. 10a). Notably, the Ce^{3+}: 4f→5d yellow-emitting and Eu^{3+}: $^5D_0 \rightarrow ^7F_2$ red-emitting can be simultaneously observed under 463 nm blue light excitation. Therefore, the YAG:Ce^{3+} and LCLSO:Eu^{3+} co-doped GC should a promising inorganic color converter to be applied in WLEDs after coupled with blue chip.

In a further experiment, to realize the tunable emitting colors, a series of GCs containing both the LCLSO:Eu^{3+} red phosphors (1~15 wt%) and the Ce: YAG yellow phosphors (3 wt%) are investigated, as shown in Fig. 10b. From the PL spectra, it can be observed that all the spectra consist of a broad yellow emission band of Ce^{3+} and a sharp red emission band of Eu^{3+}. The dominant 611 nm red emission, ascribing to $^5D_0 \rightarrow ^7F_2$ hypersensitive transition, gradually intensifies as the content of LCLSO:Eu^{3+} phosphors increasing from 1 wt% to 15 wt%. Fig. 11 shows the CIE color coordinates of the YAG:Ce^{3+} and LCLSO:Eu^{3+} co-doped GC with various LCLSO:Eu^{3+} contents (1~15 wt%) and a fixed Ce: YAG content (3 wt%). Evidently, the changes in emission spectra with different LCLSO:Eu^{3+} contents bring out rich luminescence colors for the

as-obtained GCs under UV (393 nm) and blue (463 nm) light excitation. It can be observed that the content of LCLSO:Eu^{3+} red phosphors in GC has a great influence on the position of color points in the CIE diagram. Under 463 nm light excitation, the luminescent color tends to warm light due to the increase of red component in the GC samples. As a comparison, the CIE color coordinates of the GC samples under 393 nm UV light excitation are also provided. Obviously, the tunability of luminescent color from yellow to red with increase of LCLSO:Eu^{3+} content is clearly recognized due to the strong excitation of Eu^{3+} by 393 nm UV light. To visualize the color-tunable luminescence, photographs of the corresponding GC samples, under 393 nm UV and 463 nm blue light excitation, are also provided in Fig. 11. Evidently, the modification of luminescent color of GC with increase of LCLSO:Eu^{3+} content (1~15 wt%) is clearly discerned by the naked eyes.
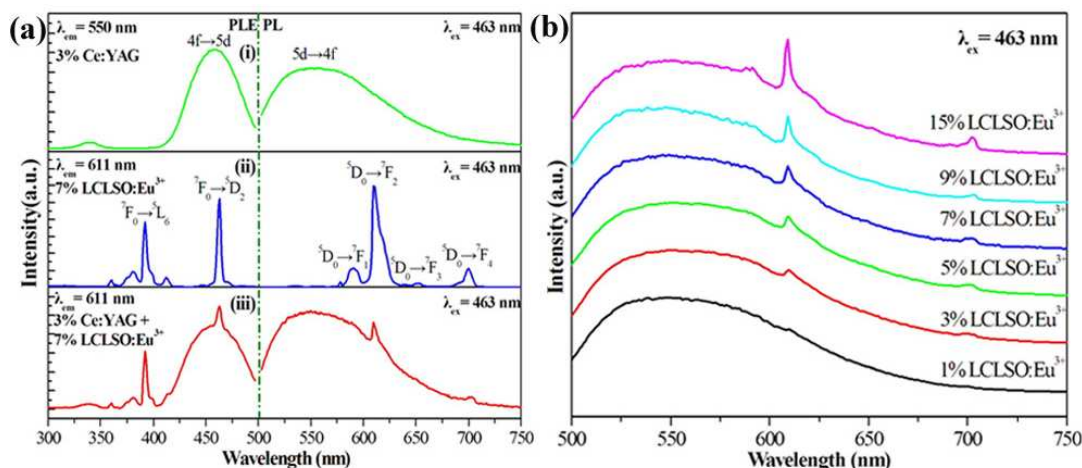
Fig. 10 (a) PLE and PL spectra for (i) the YAG:Ce^{3+} single-doped GC, (ii) LCLSO:Eu^{3+} single-doped GC, and (iii) YAG:Ce^{3+} and LCLSO:Eu^{3+} co-doped GC. (b) PL spectra of the YAG:Ce^{3+} and LCLSO:Eu^{3+} co-doped GC with various LCLSO:Eu^{3+} contents (1~15 wt%) and a fixed YAG:Ce^{3+} content (3 wt%).
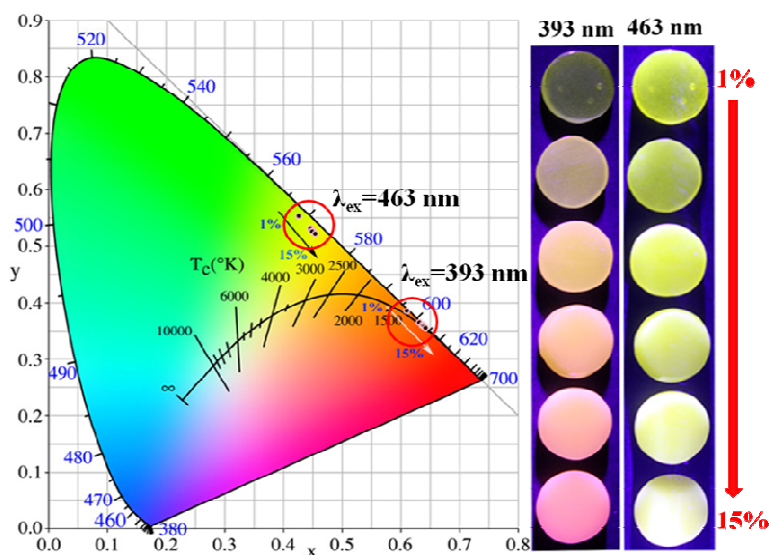
Fig. 11 CIE Color coordinates of the YAG:Ce^{3+} and LCLSO:Eu^{3+} co-doped GC with various LCLSO:Eu^{3+} contents (1~15 wt%) and a fixed Ce: YAG content (3 wt%) calculated from the emission spectra under 393 and 463 nm excitation (left). The corresponding luminescent photographs of GC samples are also provided (right).

In order to evaluate the energy transfer interactions between Ce^{3+} and Eu^{3+}, the decay behaviors of Ce^{3+} and Eu^{3+} in the co-doped GC samples were studied. The decay curves of Eu^{3+} in GCs with various LCLSO:Eu^{3+} contents are presented in Fig.12a. Although different contents of LCLSO:Eu^{3+} (1~15 wt%) have been introduced in the GC samples, the Eu^{3+} lifetimes are not obviously altered, confirming that the LCLSO:Eu^{3+} particles are not eroded by the melting glass. Furthermore, the influence of the LCLSO:Eu^{3+} content on the Ce^{3+} decay behaviors are also investigated, as shown in Fig. 12b. The lifetime in nanosecond order is one of the characteristics of Ce^{3+} electric-dipole allowed 5d→4f transition. Obviously, all the decay curves of Ce^{3+} do not vary with increase of LCLSO:Eu^{3+} doping content, indicating the Eu^{3+} has not influence on Ce^{3+} emitting in these GC samples. Therefore, it can be concluded that the energy transfers between Ce^{3+} and Eu^{3+} are highly suppressed in the present glass ceramics, which should be ascribed to the Ce^{3+} ions

locating in the YAG crystalline phase while the Eu^{3+} one locating in the LCLSO lattice. Such spatial isolation for these two active ions can effectively lessen adverse energy transfer between Ce^{3+} and Eu^{3+} (Fig. 13), leading to both intense yellow and red emissions originated from Ce^{3+} and Eu^{3+} respectively. As a consequence, the PL QY of the LCLSO:Eu^{3+} and YAG:Ce^{3+} co-doped GC is measured to be 89.3% (Fig. 14), which is approaching to the QY value of the Ce: YAG single-doped GC(93.04%).
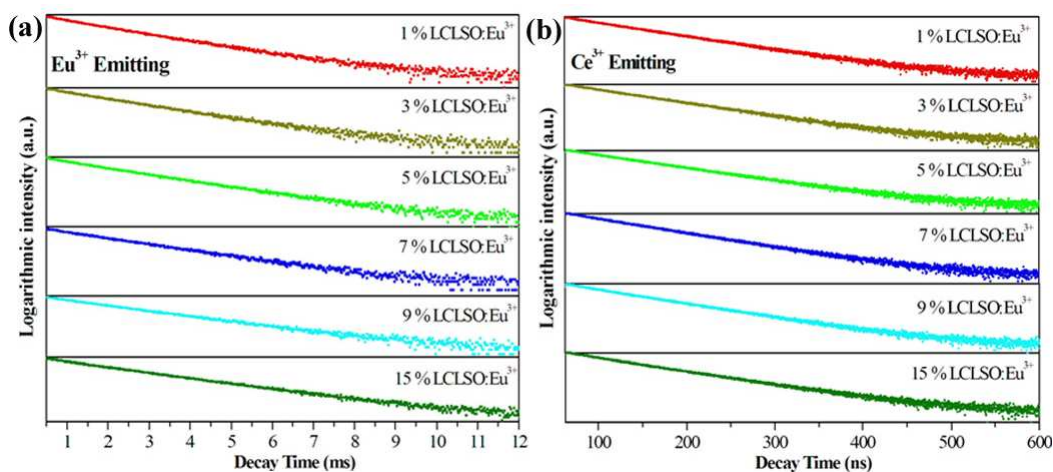
Fig. 12 Decay curves of (a) Eu^{3+}: $^{5}D_{0}$ emitting-state and (b) Ce^{3+}: 5d emitting-state in the LCLSO:Eu^{3+} (1~15 wt%) and YAG:Ce^{3+} (3 wt%) co-doped GCs.
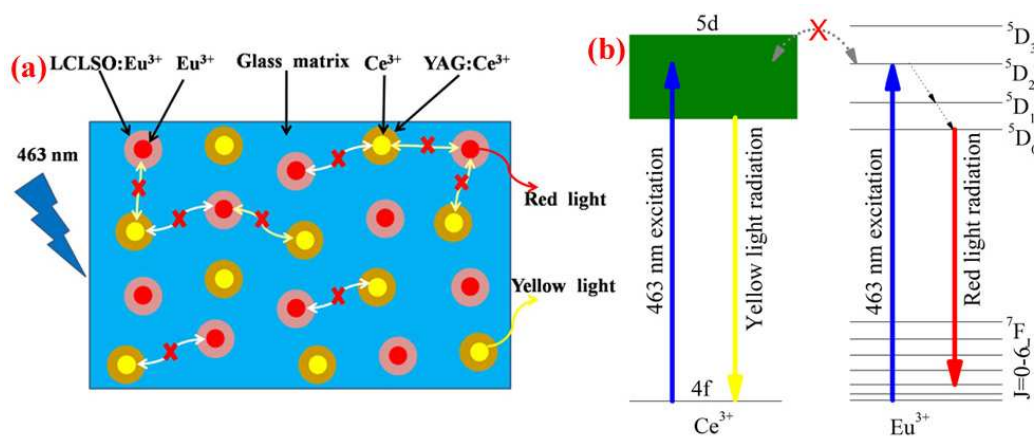
Fig. 13 (a) A sketch showing the distribution and luminescent behaviors of Ce^{3+} and Eu^{3+} ions in GC. (b) Schematic energy level diagrams of Ce^{3+} and Eu^{3+} ions showing the energy transfer cutoff between Ce^{3+} and Eu^{3+}.
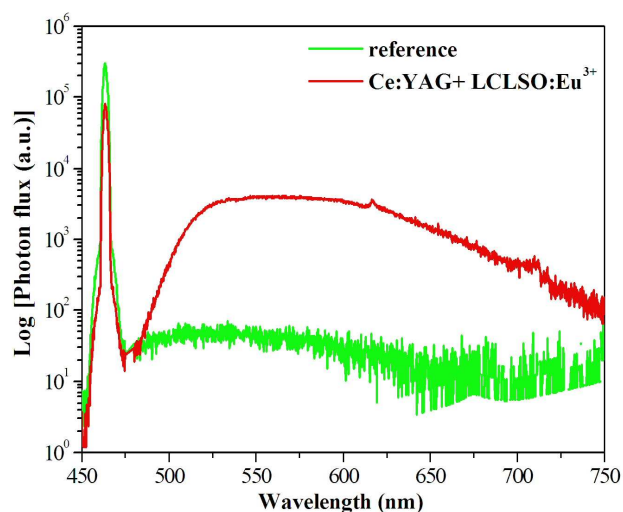
Fig. 14 Quantitative excitation and emission spectra of the LCLSO:Eu^{3+} and YAG:Ce^{3+} co-doped GC and reference sample recorded by a spectrofluoremeter equipped with an integrating sphere for QY measurement.

Finally, as a proof-of-concept experiment, the WLEDs were fabricated by encapsulating a GC disk on the InGaN blue chip to evaluate the device performance. The electroluminescent (EL) spectrum of a WLED, constructed by coupling the 7 wt% LCLSO:Eu^{3+} and 3 wt% YAG:Ce^{3+} co-doped GC with a blue LED, is demonstrated in Fig. 15. The blue emission band is attributed to the luminescence of the InGaN chip, the broad yellow emission band is ascribed to the 5d→4f transition of Ce^{3+} in the YAG, and the sharp red emission band is assigned to the $^5D_0$→$^7F_2$ transition of Eu^{3+} in LCLSO. The impact of LCLSO:Eu^{3+} content on the measured photometric and chromaticity parameters of WLEDs is tabulated in Table 2. Evidently, as the LCLSO:Eu^{3+} content increasing from 1 wt% to 15 wt%, the yielded white light gradually shifts from cool to warm (Fig. 16), the CIE color coordinate moves from (0.3149, 0.3489) to (0.3409, 0.3886), the CCT decreases from 6331K to 4936K, while the CRI increases from 70.4 to 77.9. These results indicated that the introduction of LCLSO:Eu^{3+} into the YAG:Ce^{3+} embedded GC can effectively decrease CCT and increase CRI of the GC-based WLED, resulting in the emitting of warm white-light.

Importantly, the LE of the WLEDs has not been obviously reduced with increase of

LCLSO:Eu^{3+} content. Based on these optical parameters, the optimal LCLSO:Eu^{3+}

content in the co-doped GC is found to be 7 wt%, and the corresponding GC-based

WLED has a LE of 101 lm/W, a CCT of 5449 K and a CRI of 73.7.
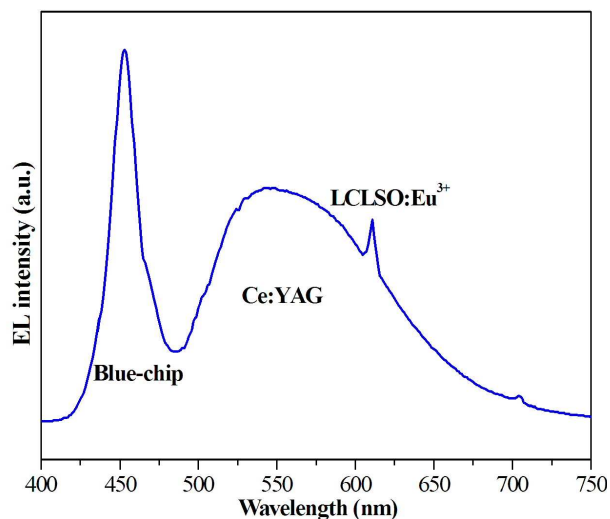
Fig. 15 EL spectrum of a WLED device fabricated by coupling the InGaN blue chip with the
LCLSO:Eu^{3+} and YAG:Ce^{3+} co-doped GC.

Table 2 Measured optical parameters of the GC-based LEDs

LCLSO:Eu^{3+} Content (wt %)	Luminous efficiency (lm/W)	CCT (K)	Ra	Chromaticity coordinate	
				X	Y
1	108.50	6331	70.4	0.3149	0.3489
3	102.26	6137	70.6	0.3187	0.3525
5	101.81	6006	71.9	0.3204	0.3542
7	101.16	5449	73.7	0.3286	0.3696
9	100.09	5376	73.9	0.3364	0.3830
15	98.51	4936	77.9	0.3409	0.3886
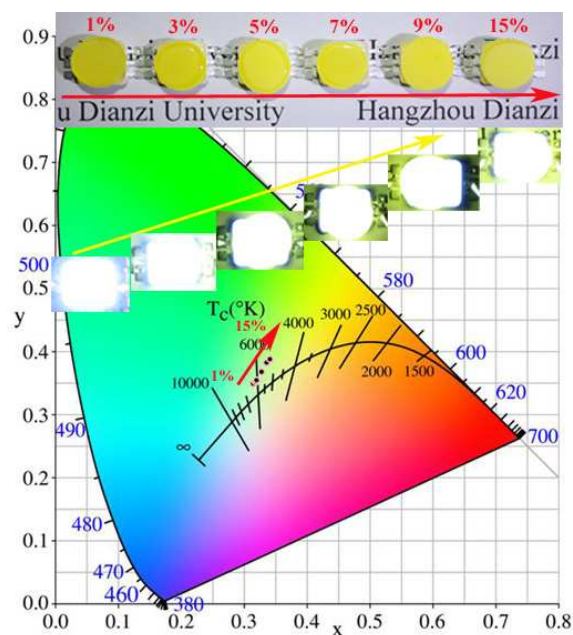
Fig. 16   Photographs and CIE chromaticity diagram of WLED devices fabricated by coupling InGaN blue chip with the 3 wt% YAG:Ce^{3+} and (1, 3, 5, 7, 9, 15) wt% LCLSO:Eu^{3+} co-doped GC.

4. Conclusions

In summary, we have developed a series of garnet-based Li$_6$CaLa$_{2-2x}$Eu$_{2x}$Sb$_2$O$_{12}$ (x=0.1~1.0) red phosphors without concentration quenching effect by a conventional solid-state method. Impressively, taking Li$_6$CaLaEuSb$_2$O$_{12}$ as an example, the phosphor exhibits excellent thermal stability with only 9.7% loss when the recording temperature increases from 293 K to 553 K, and the QY of the red phosphor reaches as high as 41.29%. Furthermore, the YAG:Ce^{3+} yellow phosphors and LCLSO:Eu^{3+} red ones co-doped glass ceramics are fabricated to explore their potential applications in high-power warm WLEDs. Owing to the low co-sintering temperature (600 $^{\circ}$C), the erosion of both yellow and red phosphor particles by the melting glass is avoided and the luminescence performance is retained. Importantly, the adverse energy transfers between Ce^{3+} and Eu^{3+} in the present glass ceramics are effectively cut off due to the spatial separation of Ce^{3+} in YAG host and Eu^{3+} in LCLSO crystal, and subsequently the QY of the co-doped GC reaches 89.3%. Finally, the investigated glass ceramics

encapsulated WLEDs exhibit tunable CCT and CRI by modifying the content of LCLSO:Eu^{3+} red phosphors, resulting in the warm white-light emitting with an optimal LE of 101 lm/W, a CCT of 5449 K and a CRI of 73.7. These results indicate that the present glass ceramic should be an excellent alternative to the conventional phosphor/silicon color converter for the construction of high-power warm WLEDs.

Acknowledgment

References

1   H. M. Zhu, C. C. Lin, W. Q. Luo, S. T Shu, Z. G. Liu, Y. S. Liu, J. T. Kong, E. Ma, Y. G. Cao, R. S. Liu and X. Y. Chen, *Nat. Commun.* 2014, **5**, 4312.

2   P. Pust, V. Weiler, C. Hecht, A. Tücks, A. S.Wochnik, A. K. Henß, D. Wiechert, C. Scheu, P. J. Schmidt and W. Schnick, *Nat. Mater.* 2014, **13**, 891.

3   Z. G. Xia, J. Zhou and Z. Y. Mao, *J. Mater. Chem. C* 2013, **1**, 5917.

4   F. Y. Wang, Y. Lin, H. L. Shi, W. C. Wang, Z. H. Deng, J. Chen, X. Y. Yuan and Y. G. Cao, *Opt. Express* 2014, **22**, A1355.

5   A. A. Setlur, *Soc. Interf.* 2009, **18**, 32.

6   H. D. Nguyen, C. C. Lin, M. H. Fang and R. S. Liu, *J. Mater. Chem. C* 2014, **2**, 10268.

7   C. H. Huang, W. R. Liu, T. S. Chan and Y.T. Lai, *Dalton Trans.* 2014, **43**, 7917.

8   C. Guo, L. Luan, C. Chen, D. Huang and Q. Su, *Mater. Lett.* 2008, **62**, 600.

9   R. Mueller-Mach and G. Mueller, *Proc. SPIE* 2000, **3938**, 30.

10   R. Mueller-Mach, G. Mueller, M.R. Krames, H.A. Höppe, F. Stadler, W. Schnick, T. Juestel and P. Schmidt, *Phys. Status Solidi* 2005, **202**, 1727.

11   K. Uheda, N. Hirosaki, Y. Yamamoto, A. Naito, T. Nakajima and H. Yamamoto, *Electrochem. Solid ST* 2006, **9**, H22.

12   L. Y. Chen, J. K. Chang, Y. R. Wu, W. C. Cheng, J. H. Chen, C. C. Tsai and W. H. Cheng, *J. Disp. Technol.* 2013, **9**, 441.

13   L. Y. Chen, W. C. Cheng, C. C. Tsai, Y. C. Huang, Y. S. Lin and W. H. Cheng, *Opt. Mater.*

Express 2014, **4**, 121.

14 S. Yi, W. J. Chung and J. Heo, *J. Am. Ceram. Soc.* 2014, **97**, 342.

15 C. C. Tsai, W. C. Cheng, J. K. Chang, L. Y. Chen, J. H. Chen, Y. C. Hsu and W. H. Cheng, *J. Disp. Technol.* 2013, **9**, 427.

16 S. Fujita, S. Yoshihara, A. Sakamoto, S. Yamamoto and S. Tanabe, *Proc. SPIE* 2005, **5941**, 594111.

17 S. Fujita, A. Sakamoto and S. Tanabe, *IEEE J. Sel. Top. Quant.* 2008, **14**, 1387.

18 S. Tanabe, S. Fujita, S. Yoshihara, A. Sakamoto and S. Yamamoto, *Proc. SPIE* 2005, **5941**, 594112.

19 R. Zhang, H. Lin, Y. L. Yu, D. Q. Chen, J. Xu and Y. S. Wang, *Laser Photonics Rev.* 2014, **8**, 158.

20 D. Q. Chen and Y. Chen, *Ceram. Int.* 2014, **40**, 15325.

21 B. Wang, H. Lin, J. Xu, H. Chen and Y. S. Wang, *ACS Appl. Mater. Inter.* 2014, **6**, 22905.

22 Y. K. Lee, Y. H. Kim, J. Heo, W. B. Im and W. J. Chung, *Opt. Lett.* 2014, **39**, 4084.

23 A. Katelnikovas, S. Sakirzanovas, D. Dutczak, J. Plewa, D. Enseling, H. Winkler, A. Kareiva and T. Jüstel, *J. Lumin.* 2013, **136**, 17.

24 R. Murugan, V. Thangadurai and W. Weppner, *Angew. Chem. Int. Edit.* 2007, **46**, 7778.

25 F. X. Liu, Y. Z. Fang, J. S. Hou, N. Zhang and Z. F. Ma, *Ceram. Int.* 2014, **40**, 3237.

26 C. Bernuy-Lopez, W. J. Manalastas, J. M. L. Amo, A. Aguadero, F. Aguesse and J. A. Kilner, *Chem. Mater.* 2014, **26**, 3610.

27 W. G. Zeier, S. L. Zhou, B. Lopez-Bermudez, K. Page and B. C. Melot, *ACS Appl. Mater. Inter.* 2014, **6**, 10900.

28 F. X. Liu, Y. Z. Fang, N. Zhang, J. S. Hou, Z. F. Ma and G. Y. Zhao, *Ceram. Int.* 2014, **40**, 14781.

29 G. J. Gao, J. X. Wei, Y. Shen, M. Y. Peng and L. Wondraczek, *J. Mater. Chem. C* 2014, **2**, 8678.

30 J. Wang, Y. Cheng, Y. L. Huang, P. Q. Cai, S. Kim and H. J. Seo, *J. Mater. Chem. C* 2014, **2**, 5559.

31 W.P. Chen, A.H. Zhou, Y. Liu, X.Y. Dai and X. Yang, *J. Solid State Chem.* 2014, **220**, 177.

32   L.D. Jing, X.H. Liu and Y.T. Li, *J. Lumin*. 2015, **158**, 351.

33   J. Awaka, N. Kijima, Y. Takahashi, H. Hayakawa and J. Akimoto, *Solid State Ionics* 2009, **180**, 602.

34   E.J. Cussen and Th.W.S. Yip, *J. Solid State Chem*. 2007, **180**, 1832.

35   G. Will, *Powder Diffraction: The Rietveld Method and the Two Stage Method to Determine and Refine Crystal Structures from Powder Diffraction Data*, Springer, Berlin, Germany, 2006

36   T. Badapanda, L. S. Cavalcante, G. E. D. Luz, N. C. Batista, S. Anwar and E. Longo, *Metall. Mater. Trans. A* 2013, **44A**, 4296.

37   R. Murugan, W. Weppner, P. Schmid-Beurmann and V. Thangadurai, *Mater. Res. Bull.* 2008, **43**, 2579.

38   W. N. Jiang, R. L. Fu, X. G. Gu, P. F. Zhang and A. Z. Coşgun, *J. Lumin.* 2015, **157**, 46.

39   H. Y. Jiao and Y. H. Wang, Phys. B 2012, **407**, 2729.

40   Y. Zhang, L. Wu, M. Y. Ji, B. Wang, Y. F. Kong and J. J. Xu, *Opt. Mater. Express* 2012, **2**, 92.

41   F. Yang, Y.J. Liang, M.Y. Liu, X.J. Li, M.F. Zhang and N. Wang, *Opt. Laser Technol.* 2013, **46**, 14.

42   Z. J. Wang, J. P. Zhong, H. B. Liang and J. Wang, *Opt. Mater. Express* 2013, **3**, 418.

43   J. Percival, D. Apperley and P.R. Slater, *Solid State Ionics* 2008, **179**, 1693.

44   G. Blasse, B.C. Grabmaier, *Luminescent Materials*, Springer-Verlag, Berlin and New York, 1994

45   S. Long, J. S. Hou, G. H. Zhang, F. Q. Huang and Y. Zeng, *Ceram. Int.* 2013, **39**. 6013.

46   Z. L. Wang, H. B. Liang, M. L. Gong and Q. Su, *J. Alloys Compd.* 2007, **432**, 308.

47   A. Huignard, T. Gacoin and J.P. Boilot, *Chem. Mater.* 2000, **12**, 1090.

48   S.Y. Zhang, Y. Nakai, T. Tsuoi, Y.L. Huang and H.J. Seo, *Chem. Mater.* 2011, **23**, 1216.

49   X. B. Qiao, Y. Cheng, L. Qin, C. X. Qin, P. Q. Cai, S. Kin and H. J. Seo, *J. Alloys Compd.* 2014, **617**, 946.

50   C. Görller-Walrand and K. Binnemans, *Phys. Chem. Rare Earths* 1996, **23**,121.

Graphic Abstract
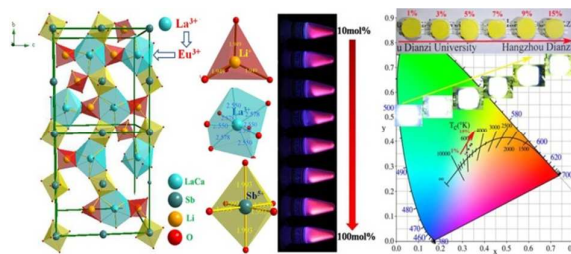
Garnet-based $Li_6CaLa_{2-2x}Eu_{2x}Sb_2O_{12}$ (x=0.1~1.0) red phosphors and the related inorganic glass ceramics were fabricated to find potential applications in WLEDs.